Bull Mater Sci (2020) 43:268
https://doi.org/10.1007/s12034-020-02236-x

Density functional study of elastic and thermal properties of cubic mercury-zinc-chalcogenide ternary alloys

MANISH DEBBARMA[1], SUBHENDU DAS[1,2], BIMAL DEBNATH[1], DEBANKITA GHOSH[1], SAYANTIKA CHANDA[1], RAHUL BHATTACHARJEE[1,3] and SURYA CHATTOPADHYAYA[1,*]

[1]Department of Physics, Tripura University, Suryamaninagar 799022, India
[2]Department of Physics, D. D. M. College, Khowai 799202, India
[3]Department of Physics, Women's College, Agartala 799001, India
*Author for correspondence (surya_ju@yahoo.com)

MS received 25 February 2020; accepted 1 April 2020

Abstract. First principle calculations of elastic and thermal properties of zinc-blende specimens within $Hg_xZn_{1-x}S$, $Hg_xZn_{1-x}Se$ and $Hg_xZn_{1-x}Te$ ternary systems are executed. Elastic stiffness constants decrease non-linearly with increasing Hg-concentration in each system. Each cubic sample is mechanically and dynamically stable, elastically anisotropic, compressible against elastic deformation, ductile and fairly plastic. Hardness of specimens in each system reduces with enhancement in Hg-composition. Mixed kind of bonding with dominancy of covalent over ionic in most cases, bond bending over stretching and central type of interatomic bonding forces are calculated. In each system, covalency, Debye temperature and frequency, Debye temperature for acoustic phonon, thermal conductivity and melting temperature of specimens decreases, while Philip ionicity and Gruneisen parameter increases with enhancing Hg-concentration.

Keywords. Mercury-zinc-chalcogenide ternary alloys; DFT; FP-LAPW; WC-GGA; elastic and thermal properties; Hg-concentration dependence of calculated properties.

1. Introduction

During the past several decades, a great deal of attention has been devoted to the study of various properties of group IIB–VIA diatomic zinc chalcogenides and mercury chalcogenides, but most of the interesting characteristics of the latter are completely diverse from other IIB–VIA semiconductors. The ambient phases of Zn-chalcogenides are either wurtzite (B4) or zinc blende (B3) [1], while the latter is one of the stable phases of Hg-chalcogenides [2–4]. Wide direct band gap Zn-chalcogenide semiconductors have diverse applications in infrared spectroscopy, fibre-optics, optical memory devices, photovoltaic devices, thin-film transistors, solid state laser devices, THz emitters, detectors and imaging systems [5–8]. Experiments have created controversy regarding inverted types of electronic band structures and negative/zero/narrow positive band gaps of diatomic Hg-chalcogenides [9–14]. They are technologically important materials in synthesizing nanostructures [15–19], in fabricating infrared (IR) detectors, lasers, thermoelectric devices, photovoltaic and solar cells [20–25].

In some important experimental studies, elastic and thermal properties of ZnS, ZnSe and ZnTe [26–31] as well as HgS, HgSe and HgTe [32–36] were investigated. Elastic constants for ZnS, ZnSe and ZnTe were measured by Berlincourt and coworkers [26]. Pressure dependences of elastic constants of ZnTe and ZnSe in single crystals at 77–300°K [27] and zinc-blende structure at 295°K [28] were investigated by Lee. Wave shock-induced phase transitions and Hugoniot elastic limits for ZnS and ZnSe were investigated by Gust [29]. Elastic constants of ZnSe at 295°K and their Brillouin frequency were measured by Hodgins and Irwin [30]. Phonon density of states and Debye temperatures for cubic ZnS and ZnTe were investigated by Vagelatos and coworkers [31]. Temperature dependence of elastic constants of cubic mercury telluride between 1.4 and 300 K were measured by Alper and Saunders [32]. Elastic constants of HgSe in the temperature range 4.2–300 K were measured by Lehoczky and coworkers [33]. Thermal expansion and heat capacity of HgTe at different low temperatures were measured by Collins and coworkers [34]. Ultrasonic wave velocities and elastic constants of HgSe as function of hydrostatic pressure were investigated by Ford and coworkers [35]. Nelson and coworkers [36] have measured thermal conductivity of HgSe from resonant phonon scattering experiment. Further, large number of experimental data on different properties of mercury and zinc chalcogenides has also been reported in several other books/literature [37–40]. In addition to the said

Published online: 08 October 2020

experiments, mechanical and thermal features of diatomic zinc chalcogenides [41–49] and mercury chalcogenides [50–58] were reported from several first principle based theoretical investigations.

In materials science, precise tuning of different physical properties of some materials as per requirement can be performed with formation of alloys by amalgamating the compounds in their identical crystallographic phase. Using this technique, elastic and thermal features of zinc-blende HgS, HgSe and HgTe can be modified by forming their $Hg_xZn_{1-x}S$, $Hg_xZn_{1-x}Se$ and $Hg_xZn_{1-x}Te$ ternary alloys, when Zn-chalcogenide unit cells are doped with Hg atom(s) at different concentrations. The growth of wide-band-gap $Hg_xZn_{1-x}Se$ (x = 0–0.14) epitaxial layers on GaAs substrate and their light emission in the visible spectral region at room temperature [59] was investigated. Moreover, thermodynamic stability of bulk and epitaxial ZnHgTe alloys with δ lattice-parameter model [60] as well as structural and optoelectronic properties of HgZnS, HgZnSe and HgZnTe with density functional FP-LAPW approach [61,62] were a few theoretical studies. Unfortunately, no experimental or theoretical study on elastic and thermal features of $Hg_xZn_{1-x}S$, $Hg_xZn_{1-x}Se$ and $Hg_xZn_{1-x}Te$ ternary alloys were performed so far.

For the first time, results from first principle calculations on mechanical and thermal properties of zinc-blende $Hg_xZn_{1-x}S$, $Hg_xZn_{1-x}Se$ and $Hg_xZn_{1-x}Te$ ternary alloys at Hg-concentrations x = 0.0, 0.25, 0.50, 0.75 and 1.0 are reported in this paper. Mechanical and thermal features of each cubic specimen are calculated in terms of respective elastic stiffness constants C_{11}, C_{12} and C_{44}. The Hg-concentration dependence of each of the said properties are also studied and reported for the specimens under each of the $Hg_xZn_{1-x}S$, $Hg_xZn_{1-x}Se$ and $Hg_xZn_{1-x}Te$ systems.

2. Method of calculations

The density functional theory (DFT) [63,64] based FP-LAPW methodology [65] is implemented successfully in practice through one of the program code WIEN2K [66], which is used to calculate different aspects of solids. To carry out calculations of elastic and thermal properties of the said specimens, cubic2-elastic program package of Jamal and coworkers [67] is used as an adjunct code of WIEN2K. The WC-GGA [68] scheme is used to compute exchange-correlation (XC) potentials for structural and mechanical properties. The graphic code XCrySDen [69] is utilized for visualization purpose in the present study.

The atoms are considered to be located within the non-overlapping muffin-tin spheres in FP-LAPW method. With maximum angular momentum l_{max} = 10 and with spherical harmonics, the expansion of Kohn–Sham wave functions are carried out inside muffin-tin spheres. In contrast, with the largest K-vector, $K_{max} = 8.0/R_{MT}$, plane wave expansion of the same are carried out in the interstitial region. The smallest muffin-tin radius R_{MT} for Hg, Zn, S, Se and Te has been selected as 2.5, 2.4, 2.1, 2.3 and 2.5 a.u., respectively, to avoid charge leakage from the core. The Brillouin zone integrations have been performed with 3000 k-points. Convergence in total energy is acquired self-consistently with an energy threshold of 10^{-5} Ry.

3. Results and discussion

3.1 *Lattice constants*

With respect to atomic positions and cell parameters of any unit cell, total energy is minimized self-consistently and hence the parabolic variation of total energy with volume is fitted to Murnaghan's equation of state [70] to obtain equilibrium lattice constant (a_0) of the cell. In table 1, calculated a_0 for all the binary and ternary specimens are reported and good agreement between calculated a_0 for binary compounds and the respective experimental a_0 for HgS, HgSe and HgTe as well as ZnS, ZnSe and ZnTe [37,39] are observed. Moreover, calculated a_0 for binary and ternary specimens are in good agreement with respective previously calculated a_0 for diatomic Zn-chalcogenides [43,47,48,61], Hg-chalcogenides [50,53,55,61] and ternary HgZnX (X = S, Se and Te) [61]. In figure 1a, non-linear enhancement in calculated a_0 of specimens with enhancement in Hg-concentration x in each system are displayed.

3.2 *Mechanical properties*

3.2a *Elastic stiffness constants, elastic compliance constants and stabilities:* The lattice symmetry in a cubic crystal leaves only three non-zero elastic stiffness constants, where longitudinal elastic behaviour is represented by C_{11} and elastic shear characteristic through C_{12} and C_{44} [71]. Elastic compliance constants S_{11}, S_{12} and S_{44} of any cubic specimen, an indicator of its elastic resistances, are obtained from its C_{11}, C_{12} and C_{44} in the following way [72]:

$$S_{11} = \frac{C_{11} + C_{12}}{(C_{11} - C_{12})(C_{11} + 2C_{12})};$$

$$S_{12} = \frac{-C_{12}}{(C_{11} - C_{12})(C_{11} + 2C_{12})};\ S_{44} = \frac{1}{C_{44}}.$$

Calculated stiffness and compliance constants are reported in table 1. With enhancement in Hg-concentration x in $Hg_xZn_{1-x}S$, $Hg_xZn_{1-x}Se$ and $Hg_xZn_{1-x}Te$ systems, non-linear decrement in each of the calculated C_{11}, C_{12} and C_{44} of specimens are displayed in figure 1b–d, respectively. In table 1, good agreement between calculated C_{11}, C_{12}, C_{44} and respective experimental data for Zn-chalcogenides [26,27], Hg-chalcogenides [32,33,35,38,40] as well as some previously calculated data for Zn-chalcogenides [43,47,48]

Table 1. Calculated a_0, elastic constants (C_{ij}), elastic compliances (S_{ij}) and shear constant (C') of the cubic specimens.

Compound	a_0 (Å)	C_{11} (GPa)	C_{12} (GPa)	C_{44} (GPa)	S_{11} (GPa^{-1})	S_{12} (GPa^{-1})	S_{44} (GPa^{-1})	C' (GPa)
ZnS	5.367 5.412[a*], 5.411[b*] 5.38[a], 5.342[b] 5.335[c], 5.383[d]	108.168 104.6[d*] 118.0[b], 123.7[c] 110.15[d]	66.278 65.3[d*] 72.0[b], 62.1[c] 63.71[d]	50.915 46.13[d*] 75.0[b], 59.7[c] 60.41[d]	0.0173	−0.0066	0.0196	20.945
$Hg_{0.25}Zn_{0.75}S$	5.534 5.545[a]	99.579	63.572	47.641	0.0200	−0.0078	0.0210	18.004
$Hg_{0.50}Zn_{0.50}S$	5.668 5.67[a]	92.173	61.028	44.911	0.0230	−0.0091	0.0223	15.573
$Hg_{0.75}Zn_{0.25}S$	5.785 5.79[a]	86.929	59.122	42.692	0.0256	−0.0104	0.0234	13.904
HgS	5.893 5.852[a*, b*] 5.90[a], 5.863[e] 5.988[f]	82.227 81.3[f*, g*] 79.3[e], 63.03[f] 22.0[h], 61.8[i]	57.391 62.2[f*, g*] 65.3[e], 46.86[f], 5.0[h], 44.9[i]	40.445 26.4[f*, g*] 49.7[e], 40.76[f] 10.4[h], 25.2[i]	0.0285 0.0433[f]	−0.0117 −0.0185[f]	0.0247 0.0245[f]	12.418 7.9 ± 0.1[i*]
ZnSe	5.644 5.67[a*], 5.669[b*] 5.667[c*] 5.65[a], 5.624[b] 5.618[c], 5.630[d]	95.169 81.0[d*] 85.9±0.03[e*] 94.0[b], 95.9[c] 82.45[d]	55.368 48.8[d*] 50.6±0.04[e*] 61.0[b], 53.6[c] 42.71[d]	44.022 44.1[d*] 40.6±0.02[e*] 64.0[b], 48.9[c] 35.5[d]	0.0184	−0.0068	0.0227	19.901
$Hg_{0.25}Zn_{0.75}Se$	5.797 5.80[a]	87.211	52.095	40.691	0.0207	−0.0078	0.0246	17.558
$Hg_{0.50}Zn_{0.50}Se$	5.931 5.94[a]	80.517	49.480	38.075	0.0233	−0.0089	0.0263	15.519
$Hg_{0.75}Zn_{0.25}Se$	6.047 6.05[a]	75.549	47.549	36.172	0.0258	−0.0100	0.0276	14.000
HgSe	6.147 6.074±0.006[a*, b*] 6.14[a]	71.47 60.8[f*] 61.0[g*] 69.00[h*] 62.2±0.1[i*] 74.5[e], 52.69[f] 50.7[g], 28.7[h]	45.996 44.6[f*] 44.0[g*] 51.05[h*] 46.4±0.4[i*] 50.7[e], 37.99[f] 43.7[g], 9.9[h]	34.532 22.3[f*] 22.0[g*] 23.073[h*] 22.7±0.1[i*] 44.1[e], 33.69[f] 30.3[g], 21.4[h]	0.0282 0.0479[f]	−0.0110 −0.0201[f]	0.0290 0.0297[f]	12.737
ZnTe	6.076 6.089[a*], 6.1037[b*] 6.10[a], 6.00[b] 6.078[d]	75.883 71.3[d*] 71.1±0.03[e*] 82.0[b], 62.95[d]	39.703 40.7[d*] 40.7±0.04[e*] 42.0[b], 40.62[d]	32.579 31.2[d*] 31.3±0.02[e*] 55.0[b], 43.16[d]	0.0206	−0.0071	0.0307	18.090
$Hg_{0.25}Zn_{0.75}Te$	6.208 6.22[a]	68.987	37.016	29.742	0.0232	−0.0081	0.0336	15.986
$Hg_{0.50}Zn_{0.50}Te$	6.324 6.33[a]	63.271	34.457	27.145	0.0257	−0.0090	0.0368	14.407

Table 1. Continued.

Compound	a_0 (Å)	C_{11} (GPa)	C_{12} (GPa)	C_{44} (GPa)	S_{11} (GPa^{-1})	S_{12} (GPa^{-1})	S_{44} (GPa^{-1})	C' (GPa)
$Hg_{0.75}Zn_{0.25}Te$	6.428 6.43[a]	58.101	32.277	25.076	0.0285	−0.0102	0.0399	12.912
HgTe	6.521 6.460[a*, b*] 6.55[a], 6.521[e] 6.662[f], 6.664[g]	54.875 59.71[a*] 53.2[f*] 53.61[g*] 53.90[j*] 57.0[e], 44.29[f] 47.8[g], 30.9[h]	31.346 41.54[a*], 36.8[f*] 36.60[g*], 37.40[j*] 43.0[e], 29.49[f] 47.1[g], 11.65[h]	23.818 22.59[a*], 20.8[f*] 21.23[g*], 20.90[j*] 25.4[e], 29.35[f] 11.7[g], 20.2[h]	0.0312 0.0483[f]	−0.0113 −0.0193[f]	0.0420 0.0341[f]	11.765 8.2[j*]

Experimental data ⇒ [a*]Ref. [37], [b*]Ref. [39], [c*]Ref. [13], [d*]Ref. [26], [e*]Ref. [27], [f*]Ref. [38], [g*]Ref. [40], [h*]Ref. [33], [i*]Ref. [35], [j*]Ref. [32].
Previous theoretical data ⇒ [a]Ref. [61], [b]Ref. [43], [c]Ref. [47], [d]Ref. [48], [e]Ref. [53], [f]Ref. [55], [g]Ref. [50], [h]Ref. [51], [i]Ref. [57].

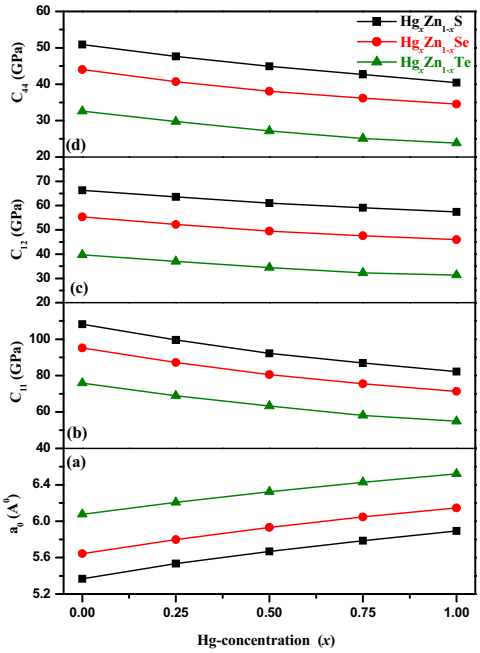

Figure 1. Concentration (x) dependence curves of calculated (**a**) a_0, (**b**) C_{11}, (**c**) C_{12} and (**d**) C_{44} of zinc-blende $Hg_xZn_{1-x}S$, $Hg_xZn_{1-x}Se$ and $Hg_xZn_{1-x}Te$ alloys.

and Hg-chalcogenides [50,51,53,55,57] are observed. In contrast, any kind of elastic stiffness constant data for ternary specimens are unavailable. Also, the $C_{11} > C_{12} > C_{44}$ trend for each specimen is observed in table 1 and aforesaid experiments on diatomic mercury and zinc chalcogenides support such trend. With enhancement in Hg-concentration x in each system, each of the S_{11}, S_{12} and S_{44} of specimens enhances marginally according to table 1. Though, elastic compliance constants for any specimen under consideration is not reported in any experimental literature, table 1 shows good agreement between computed elastic compliance constants and respective earlier theoretical data for HgS, HgSe and HgTe [55].

The Born mechanical stability criteria [73] for a cubic crystal is

$$C_{11} - C_{12} > 0;\ C_{11} + 2C_{12} > 0,\ C_{11} > 0;\ C_{44} > 0. \tag{2}$$

Each cubic specimen under consideration is mechanically stable according to table 1 due to fulfillment of aforesaid set of Born Inequalities (2).

The shear constant of any cubic crystal is [67]

$$C' = \frac{1}{2}(C_{11} - C_{12}). \tag{3}$$

According to table 1, each specimen under consideration becomes dynamically stable due to the positive sign of the respective calculated shear constant C'. With enhancement in Hg-composition x in each system, C' of specimens decreases non-linearly. Moreover, table 1 states that calculated C' for HgS and HgTe are fairly larger than the corresponding experimentally observed data for HgS [35] and HgTe [32].

3.2b *Elastic modulus and related parameters of the specimens:* The response of any crystalline material to shearing stress is indicated by its shear modulus (G). The resistance of a material to deformation upon shear stress is measured by Hill's shear modulus (G_H) [74]. The upper limit of the effective shear modulus is represented by Voigt approximation [75], while the lower limit is represented by Reuss approximation [76]. Hill's shear modulus (G_H) for cubic crystals is expressed as the arithmetic mean of Voigt shear modulus G_V and Reuss shear modulus G_R in the following way [77]:

$$G_H^A = \frac{G_V + G_R}{2}. \tag{4}$$

It can also be expressed with the geometric mean of G_V and G_R as follows [77]:

$$G_H^G = (G_V G_R)^{\frac{1}{2}}. \tag{5}$$

The G_V and G_R for a cubic crystal are calculated from its C_{11}, C_{12} and C_{44} in the following way [67]:

$$G_V = \frac{C_{11} - C_{12} + 3C_{44}}{5}, \tag{6}$$

$$G_R = \frac{5C_{44}(C_{11} - C_{12})}{4C_{44} + 3(C_{11} - C_{12})}. \tag{7}$$

In table 2, we have reported the calculated G_V, G_R, G_H^A and G_H^G. There is no such available experimental data for any of the specimens under consideration. Also, no previously calculated G_V, G_R and G_H^A for diatomic Zn-chalcogenides and ternary specimens as well as previously calculated G_H^G of any specimen under consideration is available for comparison. But in table 2, marginal overestimation of calculated G_V, G_R and G_H^A for HgS, HgSe and HgTe with respect to a couple of corresponding previously calculated data [53,55] and substantial overestimation with respect to another set of corresponding previously calculated data [51] are observed. With enhancement in Hg-composition x in each of the $Hg_xZn_{1-x}S$, $Hg_xZn_{1-x}Se$ and $Hg_xZn_{1-x}Te$ systems, non-linear decrease in each of the G_V, G_R, G_H^A and G_H^G for the compounds is presented in figure 2a–d, respectively.

As an alternative, Hashin and Shtrikman [78] proposed the upper bound G_U and the lower bound G_L of shear modulus as [77]

$$G_U = G_2 + 2\left[\frac{5}{G_1 - G_2} + \frac{18(B_0 + 2G_2)}{5G_2(3B_0 + 4G_2)}\right]^{-1}, \tag{8}$$

$$G_L = G_1 + 3\left[\frac{5}{G_2 - G_1} + \frac{12(B_0 + 2G_1)}{5G_1(3B_0 + 4G_1)}\right]^{-1}, \tag{9}$$

where $G_1 = \frac{1}{2}(C_{11} - C_{12})$ and $G_2 = C_{44}$.

The average of G_U and G_L, i.e., the Hashin–Shtrikman shear modulus (G_{HS}) has been expressed by the following relation [77]:

$$G_{HS} = \frac{(G_U + G_L)}{2}. \tag{10}$$

In table 2, we have reported the calculated G_U, G_L and G_{HS}. With the increase in Hg-concentration x in each system, a non-linear decrease in each of the G_U, G_L and G_{HS} for the specimens is presented in figure 3a–c, respectively. No experimental or previously calculated G_U, G_L and G_{HS} for any of the specimens under consideration are reported in the literature.

For a cubic crystal, bulk modulus B_0 with its C_{11} and C_{12} is expressed in the following way [67]:

$$B_0 = \frac{1}{3}(C_{11} + 2C_{12}). \tag{11}$$

In table 2, the calculated B_0 for each specimen is reported. Figure 4a shows a non-linear decrease in B_0 with increase in Hg-concentration x in each system. In table 2, good agreement between calculated B_0 of the diatomic specimens and respective experimental data for ZnS, ZnSe and ZnTe [28,37] and HgS, HgSe and HgTe [32,37,39] as well as previous theoretical data for ZnS, ZnSe and ZnTe [61,62] and HgS, HgSe and HgTe [50,51,53,55,61,62] are observed. No experimental B_0 data are available for ternary specimens, while a good agreement is observed between calculated B_0 and the respective previously calculated data [61,62]. Moreover, tables 1 and 2 confirm mechanical stability of each specimen due to their fulfillment of the condition $C_{12} < B_0 < C_{11}$ [67].

Young's modulus (Y) represents the response of a material to linear stress, where larger Y stands for better hardness and vice versa. In a crystal, it is expressed in terms of its B_0 and G_H^A in the following way [67]:

$$Y = \frac{9B_0 G_H^A}{3B_0 + G_H^A}. \tag{12}$$

In table 2, calculated Young's moduli for all the specimens are reported. With increase in Hg-concentration x in each system, non-linear decrease in calculated Y is displayed in figure 4b. No experimental Young's modulus data for any of the specimens under consideration is reported in the literature. In table 2, good agreement between calculated Y for HgS, HgSe, HgTe and some corresponding previously calculated data [51,53,55,57] is observed.

Vickers hardness (H_V) of a material can be calculated by two different empirical relationships, expressed in terms of its Hill shear modulus (G_H^A). Teter [79] proposed the first one as

$$H_V^T = 0.1769G_H^A - 2.899. \tag{13}$$

On the other hand, Chen and coworkers [80] proposed the second one as

$$H_V^C = 0.151G_H^A. \tag{14}$$

In table 2, calculated H_V^T and H_V^C are reported. With enhancement in Hg-concentration x in each system, non-linear decrease in H_V^T and H_V^C are presented in figure 4c and d, respectively, which are the same as the nature of variations of hardness in terms of B_0 or Y with x. It is also observed from table 2 that ZnS is the hardest material with the highest values of B_0, Y, H_V^T and H_V^C among all the cubic specimens under consideration, while HgTe has the lowest rigidity.

Poisson's ratio σ ($-1 \le \sigma \le 0.5$) of a material can be expressed in terms of its B_0 and G_H^A in the following way [67]:

$$\sigma = \frac{3B_0 - 2G_H^A}{2(3B_0 + G_H^A)}. \tag{15}$$

Table 2. Calculated G_V, G_R, G_H^A, G_H^G, G_L, G_U, G_{HS}, B_0, Y, H_V^T and H_V^C of cubic compounds.

Compound	G_V (GPa)	G_R (GPa)	G_H^A (GPa)	G_H^G (GPa)	G_L (GPa)	G_U (GPa)	G_{HS} (GPa)	B_0 (GPa)	Y (GPa)	H_V^T (GPa)	H_V^C (GPa)
ZnS	38.93	32.38	35.65	35.50	35.23	36.41	35.82	80.24 76.9[a*] 79.64[e], 81.10[f]	93.16	3.408	5.384
$Hg_{0.25}Zn_{0.75}S$	35.79	28.73	32.26	32.06	31.73	33.12	32.43	75.57 72.40[e], 71.37[f]	84.72	2.807	4.871
$Hg_{0.50}Zn_{0.50}S$	33.18	25.61	29.39	29.15	28.75	30.38	29.57	71.41 67.37[e], 68.56[f]	77.54	2.301	4.438
$Hg_{0.75}Zn_{0.25}S$	31.18	23.35	27.26	26.98	26.54	28.32	27.43	68.39 62.91[e], 65.68[f]	72.20	1.924	4.117
HgS	29.23 27.69[b] 9.6[d]	21.26 15.58[b], 9.5[d]	25.25 23.5[a] 21.63[b] 9.6[d]	24.93	24.45	26.36	25.41	65.67 68.6[a*] 63.6[a], 52.25[b] 35.0[d], 59.79[e] 60.67[f]	67.13 63.4[a] 57.03[b] 22.1[d] 44.1[g]	1.567	3.812
ZnSe	34.37	29.65	32.01	31.92	31.75	32.51	32.13	68.64 62.50[a*], 64.7[c*] 64.93[e], 75.68[f]	83.11	2.764	4.834
$Hg_{0.25}Zn_{0.75}Se$	31.44	26.65	29.04	28.94	28.76	29.57	29.17	63.80 60.40[e], 62.12[f]	75.65	2.239	4.385
$Hg_{0.50}Zn_{0.50}Se$	29.05	24.08	26.57	26.45	26.24	27.14	26.69	59.83 56.67[e], 57.41[f]	69.42	1.800	4.011
$Hg_{0.75}Zn_{0.25}Se$	27.30	22.14	24.72	24.59	24.36	25.35	24.85	56.88 53.51[e], 58.09[f]	64.79	1.475	3.733
HgSe	25.81 23.15[b] 6.6[d]	20.50 13.84[b] 2.5[d]	23.16 23.1[a] 18.50[b] 4.6[d]	23.00	22.75	23.82	23.28	54.49 57.6[a*] 51.66±0.2[d*] 53.93[a], 42.89[b] 44.7[c], 67.8[d] 51.17[e], 56.36[f]	60.85 61.8[a] 48.52[b] 11.8[d]	1.198	3.497
ZnTe	26.78	24.67	25.73	25.71	25.66	25.91	25.78	51.76 50.9[a*] 49.82[e], 56.11[f]	66.22	1.652	3.885
$Hg_{0.25}Zn_{0.75}Te$	24.24	22.13	23.18	23.16	23.11	23.37	23.24	47.67 47.05[e], 52.55[f]	59.85	1.202	3.501
$Hg_{0.50}Zn_{0.50}Te$	22.05	20.05	21.05	21.03	20.98	21.23	21.11	44.06 44.84[e], 46.25[f]	54.48	0.825	3.179
$Hg_{0.75}Zn_{0.25}Te$	20.21	18.21	19.21	19.19	19.13	19.40	19.27	40.89 42.56[e], 46.74[f]	49.83	0.500	2.901

Table 2. Continued.

Compound	G_V (GPa)	G_R (GPa)	G_H^A (GPa)	G_H^G (GPa)	G_L (GPa)	G_U (GPa)	G_{HS} (GPa)	B_0 (GPa)	Y (GPa)	H_V^T (GPa)	H_V^C (GPa)
HgTe	18.10 20.57[b] 8.0[d]	16.89 13.42[b], 4.4[d]	17.95 15.2[a] 17.00[b] 6.2[d]	17.92	17.86	18.16	18.01	39.19 47.6[a*,b*], 43.0[e*] 43.2[a], 34.42[b] 35.20[c], 56.8[d] 41.31[e], 43.80[f]	46.71 41.2[a] 43.78[b] 15.5[d]	0.276	2.710

Experimental data ⇒ [a*]Ref. [37], [b*]Ref. [39], [c*]Ref. [28], [d*]Ref. [35], [e*]Ref. [32].
Previous theoretical data ⇒ [a]Ref. [53], [b]Ref. [55], [c]Ref. [50], [d]Ref. [51], [e]Ref. [62], [f]Ref. [61], [g]Ref. [57].

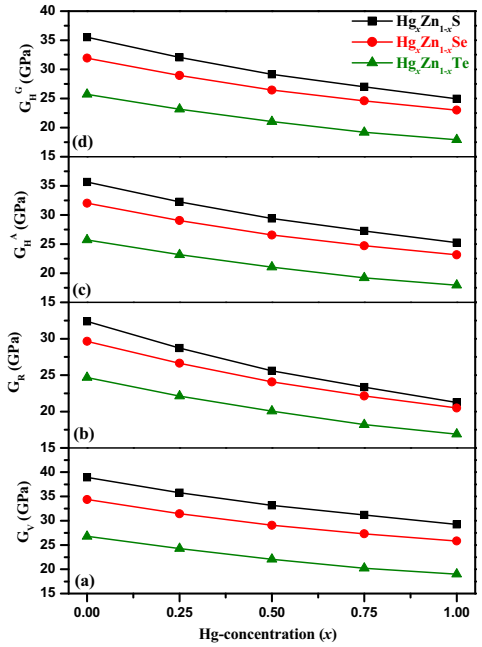

Figure 2. Concentration (x) dependence curves of calculated (**a**) G_V, (**b**) G_R, (**c**) G_H^A, (**d**) G_H^G of zinc-blende $Hg_xZn_{1-x}S$, $Hg_xZn_{1-x}Se$ and $Hg_xZn_{1-x}Te$ alloys.

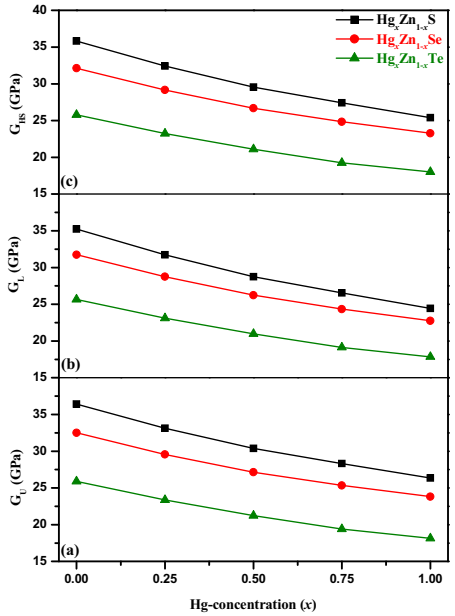

Figure 3. Concentration (x) dependence curves of calculated (**a**) G_U, (**b**) G_L, (**c**) G_{HS} of zinc-blende $Hg_xZn_{1-x}S$, $Hg_xZn_{1-x}Se$ and $Hg_xZn_{1-x}Te$ alloys.

Materials with σ close to 0.5 have an affinity towards total incompressibility [81]. The σ in between 0.25 and 0.50 indicates central nature of interatomic bonding forces in a material [81]. The σ close to 0.5 indicates better plasticity, while σ close to -1.0 indicates poor plasticity of any material. Moreover, $\sigma < 0.26$ is an indicator of brittleness, while $\sigma > 0.26$ indicates ductility of a material [81]. Table 3 shows that calculated σ for the specimens under consideration lie between 0.28 and 0.33. It indicates that each specimen under consideration shows some compressibility against elastic deformation, ductility, fair plasticity and central tendency of interatomic bonding forces. With increasing Hg-concentration x in each system, marginal increase in calculated σ are presented in figure 5a. No experimental Poisson's ratio σ for any of the specimens under consideration is reported in the literature. In contrast, fair agreement between calculated σ and respective previously calculated σ for HgS [53,55,57], HgSe and HgTe [53,55] are observed from table 3.

For a cubic crystal, Kleinmann parameter ξ ($0 \leq \xi \leq 1$) in terms of its C_{11} and C_{12} is expressed in the following way [67]:

$$\xi = \frac{C_{11} + 8C_{12}}{7C_{11} + 2C_{12}}. \tag{16}$$

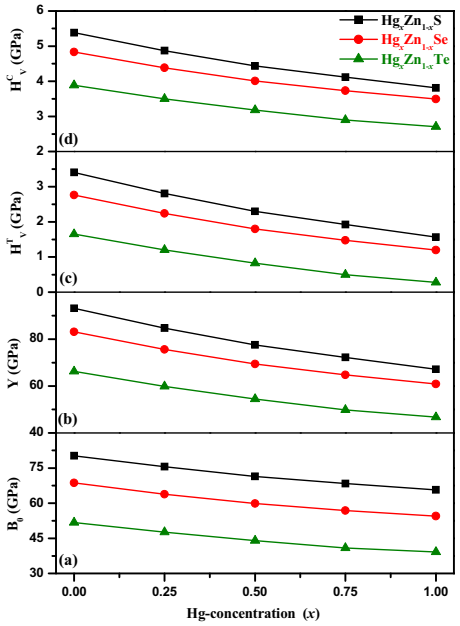

Figure 4. Concentration (x) dependence curves of calculated (**a**) B_0, (**b**) Y, (**c**) H_V^T, (**d**) H_V^C of zinc-blende $Hg_xZn_{1-x}S$, $Hg_xZn_{1-x}Se$ and $Hg_xZn_{1-x}Te$ alloys.

The $\xi = 0$ stands for minimum bond bending, while $\xi = 1$ stands for minimum bond stretching in a crystal [82]. In table 3, the calculated ξ for the specimens under consideration in between 0.64 and 0.79 point to significantly dominating bond bending over stretching in each specimen. With enhancement in Hg-concentration x in each system, non-linear enhancement in ξ of specimens are presented in figure 5b. No experimental ξ for any of the specimens under consideration is reported in the literature. In contrast, table 3 shows that calculated ξ for HgS, HgSe and HgTe are much higher than respective previously calculated data [51].

The ratio between bulk modulus (B_0) and C_{44} is an indicator of plasticity in a material [83] and calculated B_0/C_{44} for the specimens under consideration are reported in table 3. The calculated B_0/C_{44} for each of these materials, greater than unity, indicates fair plasticity of each specimen. With increasing Hg-concentration x in each system, non-linear increase in B_0/C_{44} and hence plasticity of specimens are displayed in figure 5c. No experimental or previously calculated B_0/C_{44} data for any of the specimens under consideration is reported in the literature.

Table 3. Calculated σ, ζ, B_0/C_{44}, B_0/G_H^A, C'', A_z, A_G and A_e of zinc-blende specimens.

Compound	σ	ζ	B_0/C_{44}	B_0/G_H^A	C'' (GPa)	A_z	A_G	A_e
ZnS	0.3065	0.7175	1.576	2.251	15.363	2.431	0.092	0.941
$Hg_{0.25}Zn_{0.75}S$	0.3132	0.7379	1.586	2.343	15.931	2.646	0.109	0.957
$Hg_{0.50}Zn_{0.50}S$	0.3190	0.7564	1.590	2.429	16.117	2.884	0.129	0.974
$Hg_{0.75}Zn_{0.25}S$	0.3241	0.7704	1.602	2.508	16.430	3.071	0.144	0.982
HgS	0.3296	0.7842	1.624	2.601	16.946	3.257	0.158	0.984
	0.348[a]	0.378[c]		>1.75[a]		7.10[a]		
	0.318[b]			2.42[b]		2.98[d]		
	0.154[c]							
	0.33[d]							
ZnSe	0.2982	0.6926	1.559	2.144	11.346	2.212	0.074	0.925
$Hg_{0.25}Zn_{0.75}Se$	0.3024	0.7052	1.568	2.197	11.404	2.318	0.082	0.933
$Hg_{0.50}Zn_{0.50}Se$	0.3066	0.7189	1.571	2.252	11.405	2.454	0.094	0.946
$Hg_{0.75}Zn_{0.25}Se$	0.3102	0.7307	1.573	2.301	11.377	2.584	0.104	0.958
HgSe	0.3139	0.7419	1.578	2.353	11.464	2.711	0.115	0.966
	0.337[a]	0.154[c]		>1.75[a]		5.25[a]		
	0.311[b]			2.32[b]				
	0.132[c]							
ZnTe	0.2868	0.6445	1.589	2.012	7.124	1.801	0.041	0.859
$Hg_{0.25}Zn_{0.75}Te$	0.2908	0.6556	1.603	2.056	7.274	1.861	0.046	0.861
$Hg_{0.50}Zn_{0.50}Te$	0.2939	0.6622	1.623	2.093	7.312	1.884	0.047	0.863
$Hg_{0.75}Zn_{0.25}Te$	0.2969	0.6712	1.630	2.128	7.201	1.942	0.052	0.865
HgTe	0.3014	0.6840	1.645	2.184	7.528	2.025	0.059	0.868
	0.355[a]	0.143[c]		2.8[a]		3.63[a]		
	0.288[b]			2.02[b]				
	0.249[c]							

Previous theoretical data ⇒ [a]Ref. [53], [b]Ref. [55], [c]Ref. [51], [d]Ref. [57].

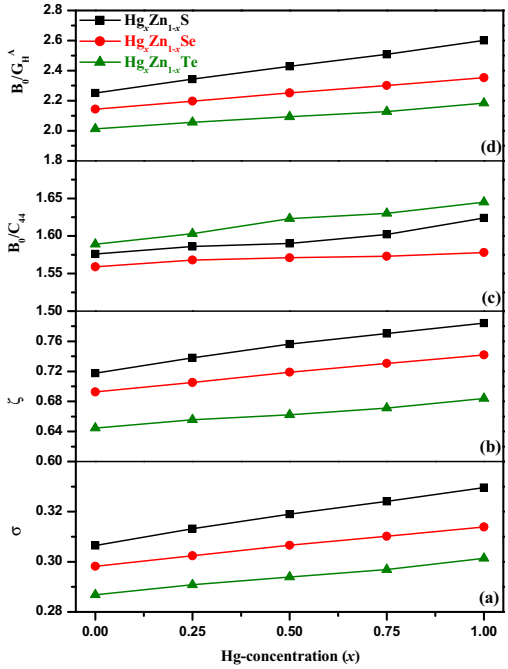

Figure 5. Concentration (x) dependence curves of calculated (**a**) σ, (**b**) ζ, (**c**) B_0/C_{44}, (**d**) B_0/G_H^A of zinc-blende $Hg_xZn_{1-x}S$, $Hg_xZn_{1-x}Se$ and $Hg_xZn_{1-x}Te$ alloys.

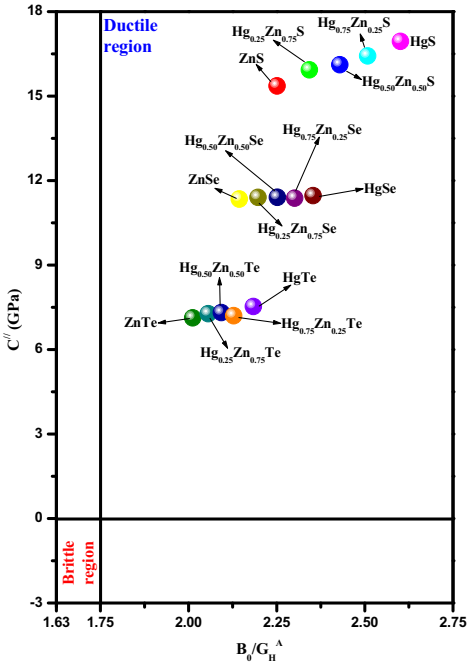

Figure 6. Correlation between Cauchy pressure C'' and Pugh's ratio B_0/G_H^A for ductility of zinc-blende specimens within $Hg_xZn_{1-x}S$, $Hg_xZn_{1-x}Se$ and $Hg_xZn_{1-x}Te$ systems.

The Pugh's ratio B_0/G_H^A [84] and Cauchy pressure $C'' = C_{12} - C_{44}$ [85] are widely used to determine ductility/brittleness of any material. The $B_0/G_H^A = 1.75$ is a threshold separating the ductile and brittle materials, where $B_0/G_H^A > 1.75$ stands for ductility and $B_0/G_H^A < 1.75$ for brittleness of a material. The positive C'' indicates ductile, while negative C'' indicates brittle materials. In table 3, evaluated B_0/G_H^A and C'' for each specimen under consideration are reported, where $B_0/G_H^A > 2$ and positive sign of C'' indicate each specimen as a ductile material. The HgS shows maximum ductility, while ZnTe shows minimum ductility among all the specimens under consideration with B_0/G_H^A as 2.601 and 2.012, respectively. No experimental B_0/G_H^A and C'' data as well as no previously calculated C'' for any of the specimens under consideration is reported in the literature. But, a couple of earlier theoretical studies [53,55] have supported $B_0/G_H^A > 1.75$ for HgS, HgSe and HgTe. Also, their calculated B_0/G_H^A are in fair agreement with corresponding previously calculated data [55]. With increase in Hg-composition x in each system, non-linear enhancement in ductility of specimens in terms of calculated B_0/G_H^A are displayed in figure 5d. Figure 6, presenting the correlations between C'' and B_0/G_H^A of all compounds within three systems, confirms that all the concerned specimens reside well inside the ductile region.

3.2c *Isotropy/anisotropy of the specimens:* Elastic anisotropy of a crystal indicates different nature of bonding in different directions in the crystal. It is also correlated with possibility of existence of microcracks in the material. In crystal physics and engineering, elastic isotropy/anisotropy in a crystal is determined by Zener anisotropy factor [67]

$$A_z = \frac{2C_{44}}{C_{11} - C_{12}}. \tag{17}$$

Uniform deformations along the three directions and hence elastic isotropy in a crystal is indicated by $A_z = 1$. In contrast, departure of A_z from unity indicates varying degrees of elastic anisotropy with maximum rigidity along $\langle 111 \rangle$ cube diagonal by $A_z > 1$ and along $\langle 100 \rangle$ cube axes by $A_z < 1$ [67]. In table 3, $A_z > 1.8$ for each specimen confirms maximum rigidity along $\langle 111 \rangle$ cube diagonal. With enhancement in Hg-concentration x in each system, non-linear increment in A_z of specimens are displayed in figure 7a. The calculated A_z for HgS is in fair agreement with previously calculated data [57], while calculated A_z for HgS, HgSe and HgTe is much lower than respective previously calculated data, obtained from another theoretical study [53].

The percentage of elastic anisotropy in a crystal is expressed in terms of G_V and G_R in the following way [86]:

$$A_G = \frac{G_V - G_R}{G_V + G_R}. \tag{18}$$

In expression (18), $A_G = 0$ represents perfect-elastic isotropy in a crystal. In contrast, the departure from zero implies elastic anisotropy with $A_G = 1$, which represents 100% anisotropy in a crystal. Anisotropy of the elastic

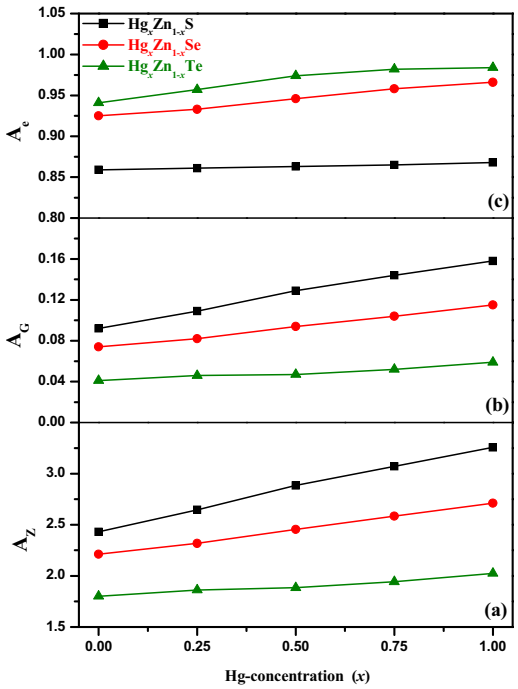

Figure 7. Concentration (x) dependence curves of calculated (**a**) A_z, (**b**) A_G, (**c**) A_e of zinc-blende $Hg_xZn_{1-x}S$, $Hg_xZn_{1-x}Se$ and $Hg_xZn_{1-x}Te$ alloys.

wave velocity (A_e) is also used to measure elastic anisotropy in a cubic crystal. The $A_e = 0$ stands for perfectly elastically isotropic, while departure from zero implies elastically anisotropic crystal. For a cubic crystal, A_e can be expressed in terms of C_{11}, C_{12} and C_{44} in the following way [86]:

$$A_e = \frac{2C_{44} + C_{12}}{C_{11}} - 1. \tag{19}$$

In table 3, we have reported the calculated A_G and A_e for the specimens under consideration. Calculated A_G for the specimens in the range 0.041–0.158 and calculated A_e in the range 0.859–0.984, indicate elastic anisotropy in all the specimens under consideration. With increase in Hg-composition x in each system, non-linear increase in A_G and A_e of specimens are shown in figure 7b and c, respectively.

The elastic isotropy/anisotropy in a crystal can also be determined from its Voigt's shear modulus (G_V), Reuss' shear modulus (G_R) and Hill's shear modulus (G_H^A). The $G_V = G_R = G_H^A$ is the criteria for elastic isotropy in a cubic crystal, but anisotropy is indicated by violation of this condition. Table 2 confirms elastic anisotropy of each of our cubic crystals due to $G_V \neq G_R \neq G_H^A$ for each of them.

Hershey [87] suggested that an isotropic material should satisfy the following cubic equation in G_H^A [81]:

$$G_H^{A^3} + \alpha G_H^{A^2} + \beta G_H^A + \gamma = 0. \tag{20}$$

The coefficients α, β and γ for a cubic specimen are expressed in terms of respective C_{11}, C_{12} and C_{44} in the following way [81]:

$$\left.\begin{aligned} \alpha &= \frac{5C_{11} + 4C_{12}}{8}, \\ \beta &= -\frac{C_{44}(7C_{11} - 4C_{12})}{8}, \\ \gamma &= -\frac{C_{44}(C_{11} - C_{12})(C_{11} + 2C_{12})}{8}. \end{aligned}\right\} \tag{21}$$

It is found that each cubic crystal under the three systems with respective set of α, β, γ and G_H^A does not satisfy equation (20). It is again indicated that each of the concerned cubic specimens is elastically anisotropic in nature.

In any crystal, elastic isotropy/anisotropy can also be examined by Lame constants λ and μ, where $\lambda = C_{12}$, and $\mu = C' = C_{44}$ are the criterion for isotropy in a crystal [67]. Lame constants for a crystal are expressed with its Y and σ in the following way [67]:

$$\lambda = \frac{Y\sigma}{(1+\sigma)(1-2\sigma)}, \tag{22}$$

$$\mu = \frac{Y}{2(1+\sigma)}. \tag{23}$$

In table 4, calculated λ and μ are reported for each of the specimens under consideration. Comparing tables 1 and 4, infringement of conditions of isotropy are observed and hence each of the specimens under consideration is elastically anisotropic in nature. With enhancement in Hg-composition x in each system, table 4 shows reduction in λ and μ of the specimens. It is also observed from table 4 that λ and μ of each of the HgS, HgSe and HgTe are substantially larger than the respective previously calculated data [51].

3.2d *Ionicity/covalency and bonding characteristics:* The correlation between the elastic constant ratio C_{11}/C_{12} and ionicity in any zinc-blende crystal was proposed by Potter [88]. The ratio C_{11}/C_{12} determines ionic/covalent/mixed nature of bonding in any zinc-blende specimen. A zinc-blende specimen contains purely ionic bonds when $C_{11}/C_{12} = 1.0$, but $C_{11}/C_{12} = 2.0$ indicates purely covalent nature of bonding in that specimen [88]. In contrast, mixed character of bonding in a zinc-blende specimen is indicated by C_{11}/C_{12} in between 1.0 and 2.0. In table 4, calculated elastic constant ratio C_{11}/C_{12} for each of the specimens under consideration is presented. The calculated C_{11}/C_{12} lies between 1.43 and 1.92 and hence mixed nature of bonding is observed in each of our specimens. The calculated C_{11}/C_{12} for each of the specimens, except $Hg_{0.75}Zn_{0.25}S$ and HgS, above 1.50 indicates that covalent bonding dominates over ionic bonding in each of these specimens. In case of $Hg_{0.75}Zn_{0.25}S$ and HgS, the calculated C_{11}/C_{12}, slightly below 1.50, indicate that ionic bonding slightly dominates over covalent bonding in each of them. The maximum domination of covalent nature is observed in

Table 4. Calculated λ, μ, C_{11}/C_{12}, Z/Z_0, α_C and f_i of zinc-blende specimens.

Compound	λ (GPa)	μ (GPa)	C_{11}/C_{12}	Z/Z_0	α_C	f_i
ZnS	56.472	35.654	1.632 1.49[a*]	0.381	0.590	0.652 0.623[e*]
$Hg_{0.25}Zn_{0.75}S$	54.070	32.256	1.566	0.431	0.564	0.671
$Hg_{0.50}Zn_{0.50}S$	51.814	29.393	1.510	0.477	0.539	0.686
$Hg_{0.75}Zn_{0.25}S$	50.215	27.264	1.470	0.511	0.521	0.704
HgS	48.840 4.3[a]	25.245 9.6[a]	1.433	0.544 0.58[d*]	0.502	0.713 0.79[d*], 0.73[b]
ZnSe	47.295	32.010	1.719	0.318	0.622	0.613 0.676[e*]
$Hg_{0.25}Zn_{0.75}Se$	44.439	29.043	1.674	0.350	0.606	0.633
$Hg_{0.50}Zn_{0.50}Se$	42.116	26.565	1.627	0.384	0.588	0.654
$Hg_{0.75}Zn_{0.25}Se$	40.400	24.724	1.589	0.414	0.573	0.672
HgSe	39.049 6.7[a]	23.157 4.6[a]	1.554 1.35±0.01[a*]	0.441 0.62[a*], 0.64[d*]	0.558	0.688 0.68[d*], 0.62[b] 0.76[c]
ZnTe	34.611	25.729	1.911	0.200	0.683	0.534 0.546[e*]
$Hg_{0.25}Zn_{0.75}Te$	32.218	23.183	1.864	0.227	0.669	0.553
$Hg_{0.50}Zn_{0.50}Te$	30.027	21.051	1.836	0.243	0.660	0.564
$Hg_{0.75}Zn_{0.25}Te$	28.077	19.212	1.800	0.265	0.649	0.579
HgTe	27.225 6.2[a]	17.945 6.2[a]	1.751 1.41[a*]	0.297 0.565[a*], 0.65[b*] 0.60[c*], 0.62[d*]	0.633	0.600 0.65[d*], 0.60[b] 0.816[c]

Experimental data ⇒ [a*]Ref. [33], [b*]Ref. [32], [c*]Ref. [89], [d*]Ref. [90], [e*]Ref. [91].
Previous theoretical data ⇒ [a]Ref. [51], [b]Ref. [53], [c]Ref. [50].

ZnTe. With enhancement in Hg-chalcogen composition x in each system, decrease in elastic constant ratio C_{11}/C_{12} and hence domination of covalent bonding over ionic bonding in specimens are presented in figure 8a. In table 4, it is clear that our calculated C_{11}/C_{12} for ZnS, HgSe and HgTe are overestimated marginally by 0.142, 0.204 and 0.341, respectively, with respect to the corresponding experimental data [33].

The relation between the elastic constant ratio C_{11}/C_{12} and the ionic charge Z/Z_0 for any zinc-blende lattice can be expressed as [88]

$$\frac{Z}{Z_0} = \left[\frac{1}{1.65}\left(\frac{C_{11}}{C_{12}} - 2.65\right)\right]^2. \quad (24)$$

In table 4, we have reported the calculated ionic charge Z/Z_0 for the specimens within $Hg_xZn_{1-x}S$, $Hg_xZn_{1-x}Se$ and $Hg_xZn_{1-x}Te$ systems. The trend of variations of Z/Z_0 with x is opposite to the corresponding variation of C_{11}/C_{12} with x in each system according to equation (24). Clearly, Z/Z_0 decreases with increase in C_{11}/C_{12}, which implies $Z/Z_0 = 1.0$ for any perfectly ionic specimen and it falls to 0.155 for any perfect covalent specimen. From table 4, we have observed that our calculated Z/Z_0 for all the specimens lie in the range 0.20–0.54 and it again confirms that each of our specimens contains mixed type of bonding. For all the specimens except $Hg_{0.75}Zn_{0.25}S$ and HgS, the calculated Z/Z_0 below 0.50 indicates that covalent bonding dominates ionic bonding in these specimens. In case of $Hg_{0.75}Zn_{0.25}S$ and HgS, calculated Z/Z_0, slightly greater than 0.50, again indicates that ionic bonding slightly dominates over covalent bonding in each of them. With enhancement in Hg-chalcogen composition x in each system, increase in calculated Z/Z_0 and hence decrease in covalency are displayed in figure 8b. According to table 4, our calculated Z/Z_0 for HgS shows excellent agreement with the corresponding experimental data [90], while that for HgSe and HgTe are underestimated fairly with respect to the corresponding experimental data for HgSe [33,89] and HgTe [32,33,89,90]. The correlation between Z/Z_0 and C_{11}/C_{12} are presented in figure 9, which again indicates that Z/Z_0 decreases with increase in C_{11}/C_{12} and vice versa.

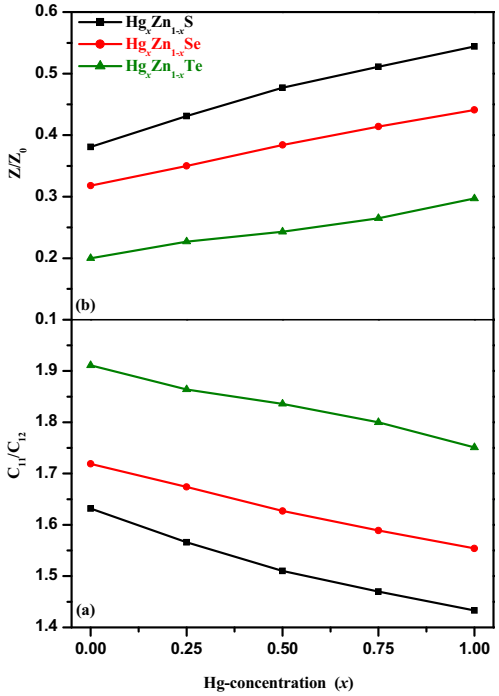

Figure 8. Concentration (x) dependence curves of calculated (**a**) C_{11}/C_{12}, (**b**) Z/Z_0 of zinc-blende $Hg_xZn_{1-x}S$, $Hg_xZn_{1-x}Se$ and $Hg_xZn_{1-x}Te$ alloys.

Based on bond-orbital model, the relations of covalency α_C with elastic stiffness constants C_{11}, C_{12} and C_{11}/C_{12} are [72]:

$$C_{11} = B_0(1+\alpha_C^2),\ C_{12} = B_0\left(\frac{2-\alpha_C^2}{2}\right) \text{ and } \frac{C_{12}}{C_{11}} = \left(\frac{2-\alpha_C^2}{2+2\alpha_C^2}\right). \quad (25)$$

With covalency α_C, the Philips ionicity factor f_i for any cubic crystal can be calculated with the following relation [72]:

$$f_i = 1-\alpha_C^2. \quad (26)$$

In table 4, calculated α_C and f_i for the cubic specimens within $Hg_xZn_{1-x}S$, $Hg_xZn_{1-x}Se$ and $Hg_xZn_{1-x}Te$ systems are listed. With increase in Hg-concentration x in each system, decrease in α_C, but increase in f_i are observed in figure 10a and b, respectively. For any specimen under consideration, no experimental α_C is available for comparison. On the other hand, our calculated f_i for ZnS, ZnSe, ZnTe, HgS, HgSe and HgTe are in close agreement with the corresponding experimental data for ZnS, ZnSe and ZnTe [91] as well as HgS, HgSe and HgTe [90]. Also, our calculated f_i for HgS and HgTe are in excellent agreement with respective previously calculated data for HgS and HgTe [53], while the f_i for HgSe lies between two corresponding previously calculated data [50,53].

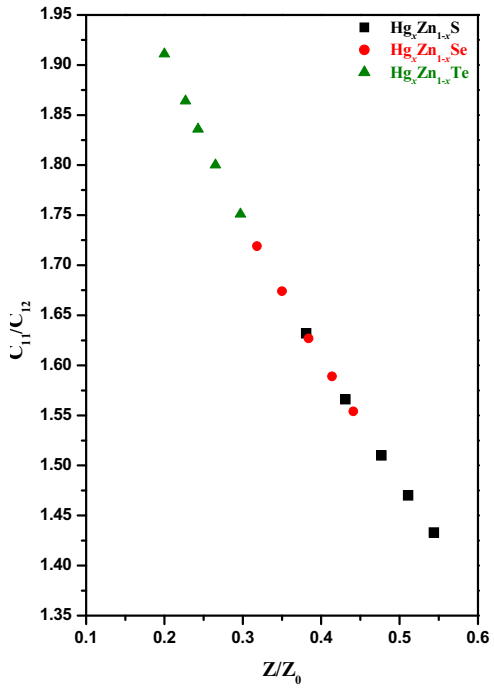

Figure 9. Correlation between C_{11}/C_{12} and Z/Z_0 for ionicity of all the zinc-blende specimens within $Hg_xZn_{1-x}S$, $Hg_xZn_{1-x}Se$ and $Hg_xZn_{1-x}Te$ systems.

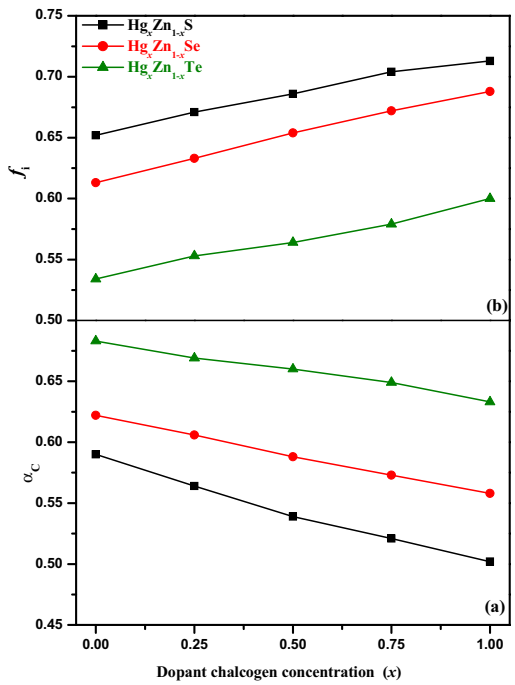

Figure 10. Concentration (x) dependence curves of calculated (**a**) α_C, (**b**) f_i of zinc-blende $Hg_xZn_{1-x}S$, $Hg_xZn_{1-x}Se$ and $Hg_xZn_{1-x}Te$ alloys.

3.2e *Sound velocity, Debye temperature, Debye frequency and Grüneisen parameter of the specimens:* The behaviour of phonons between quantum mechanical and classical regimes in a solid can be distinguished by its Debye temperature θ_D (Kelvin) and it is the approximate temperature limit below which quantum effects is observed in a solid. In a crystal, it is the temperature of maximum normal mode of vibration and indicates the correlation between the elastic features and thermodynamic properties of the crystal. If $T > \theta_D$, all modes of vibration have constant energy K_BT. On the other hand, the high-frequency modes of vibration are considered to be frozen and the acoustic vibrations are solely responsible for vibrational excitations in the temperature regime $T < \theta_D$. Therefore, θ_D for a solid in such a situation can be calculated from its elastic stiffness constants. Debye temperature for a solid is dependent on its average sound velocity (v_m). The expression for mean sound velocity v_m is [92]

$$v_m = \left[\frac{1}{3}\left(\frac{2}{v_t^3} + \frac{1}{v_l^3}\right)\right]^{-\frac{1}{3}} \tag{27}$$

Here, v_m is expressed in terms of longitudinal velocity (v_l) and transverse velocity (v_t) of sound wave. With the help of estimated G_H^A and B_0, the v_l and v_t can be expressed with the help of the following Navier equations [92]:

$$v_l = \left[\frac{B_0 + \frac{4}{3}G_H^A}{\rho}\right]^{\frac{1}{2}}, \tag{28}$$

$$v_t = \left(\frac{G_H^A}{\rho}\right)^{\frac{1}{2}}. \tag{29}$$

In the temperature regime $T < \theta_D$, we have calculated θ_D for the specimens under consideration in terms of the respective average sound velocity (v_m) using the classical relation [92]

$$\theta_D = \frac{h}{k_B}\left[\frac{3n}{4\pi}\left(\frac{N_a\rho}{M}\right)\right]^{\frac{1}{3}} v_m. \tag{30}$$

Here, h is the Planck's constant, K_B is the Boltzmann constant, n is the number of atoms in the unit cell, N_a is the Avogadro number, ρ is the density and M is the molecular weight.

In table 5, the calculated V_0, ρ, v_l, v_t, v_m and θ_D for each of the specimens under consideration have been reported. With increase in Hg-concentrations x for the $Hg_xZn_{1-x}S$, $Hg_xZn_{1-x}Se$ and $Hg_xZn_{1-x}Te$ systems, non-linear decrease in each of the v_l, v_t and v_m of the specimens are presented in figure 11a–c, respectively. Any experimental v_l, v_t and v_m for the specimens under consideration is unavailable for comparison. In contrast, calculated v_l for HgS, HgSe and HgTe are in good agreement with respective previously calculated data for HgS [55], HgSe [51] and HgTe [55]. Calculated v_t for HgS, HgSe and HgTe are also in fair agreement with respective previously calculated data for HgS, HgSe and HgTe [55]. In case of calculated v_m for HgS and HgTe, excellent agreement is observed between our calculated data and the respective data, reported from a previous theoretical study [55].

It is also observed that high Debye temperature in a solid indicates strong interatomic force and vice versa [93]. With increase in Hg-concentration x in each system, non-linear decrease in θ_D of the specimens and hence strength of bond in specimens are presented in figure 12a. Moreover, the highest value of Debye temperature for ZnS reveals that the cubic ZnS has the strongest bond and is the stiffest among all the compounds, while the reverse is observed in HgTe. No experimental θ_D for the specimens under consideration except HgSe and HgTe is available for comparison. Our calculated θ_D for HgSe and HgTe are fairly overestimated with respect to corresponding experimental data for HgSe [33,38] and HgTe [32,38]. Moreover, calculated θ_D for HgS, HgSe and HgTe are in fair agreement with respective previously calculated data for HgS [55,57], HgSe [50,55] and HgTe [50,55].

The Debye temperature θ_D also helps us to determine the frequency of maximum vibrations of atoms in a solid during a thermal transfer, known as Debye frequency ω_D. It can be expressed as [94]

$$\omega_D = \frac{k_B.\theta_D}{h}. \tag{31}$$

In table 5, calculated Debye frequency ω_D (THz) for each of the specimens within $Hg_xZn_{1-x}S$, $Hg_xZn_{1-x}Se$ and $Hg_xZn_{1-x}Te$ systems are reported. With increase in Hg-concentration x in each system, non-linear decrease in ω_D of the specimens are presented in figure 12b.

According to Debye theory of solids, the Debye temperature for an acoustic phonon (θ_a) in a solid can also be obtained from its θ_D in the following way [92]:

$$\theta_a = \theta_D n^{-\frac{1}{3}}. \tag{32}$$

In table 5, calculated θ_a (K) for each specimen under consideration are reported. With increase in Hg-concentration x in each system, non-linear decrease in θ_a of specimens are presented in figure 13a.

Grüneisen parameter (γ_a) of a solid is related to its lattice vibrations and characterizes relationship between phonon frequency and volume change [95]. The non-linear acoustical properties of a solid are related to its elastic non-linearity *via* anharmonicity in interatomic/intermolecular interactions. The anharmonicity in interactions between atoms/molecules in a solid is estimated with the help of its γ_a. Physical characteristics like thermal expansion, thermal conduction, absorption of acoustic waves, temperature dependence of elastic properties are controlled by this quantity and it reflects the peculiarity of the phonon spectrum in crystal [96]. The Grüneisen parameter (γ_a) of a solid is obtained from the expressions for sound velocities v_l and v_t in the following way [96]:

$$\gamma_a = \frac{9(V_l^2 - \frac{4}{3}V_t^2)}{2(V_l^2 + 2V_t^2)}. \tag{33}$$

Table 5. Calculated V_0, ρ, v_t, v_l, v_m, θ_D, θ_a, ω_D, γ_a, $K_{\min}$ and T_m for zinc-blende binary and ternary specimens.

Compound	V_0 (Å^3)	$\rho \times 10^3$ (kg m^{-3})	v_t (m s^{-1})	v_l (m s^{-1})	v_m (m s^{-1})	θ_D (K)	θ_a (K)	ω_D (THz)	γ_a	$K_{\min}$ (W m^{-1} K^{-1})	T_m (K)
ZnS	154.59	4.186	2918	5524	3262	574	287	11.974	1.814	1.576	1192
$Hg_{0.25}Zn_{0.75}S$	169.48	5.143	2504	4801	2802	478	239	9.974	1.857	1.273	1141
$Hg_{0.50}Zn_{0.50}S$	182.09	6.020	2209	4286	2474	412	206	8.599	1.897	1.072	1097
$Hg_{0.75}Zn_{0.25}S$	193.60	6.821	1999	3918	2240	366	183	7.627	1.932	0.931	1066
HgS	204.65	7.550	1828	3627	2050	328	164	6.854	1.973	0.822	1038
			1733[a]	3356[a]	1940[a]	306.21[a]					1723[a*]
			1481[b]	2315[b]	350[b]	76.532[b]					
			1517[c]	3193[c]	1707[c]	213[c]					
ZnSe	179.79	5.332	2450	4569	2736	458	229	9.550	1.762	1.195	1115
$Hg_{0.25}Zn_{0.75}Se$	194.81	6.073	2186	4108	2443	398	199	8.303	1.788	1.012	1068
$Hg_{0.50}Zn_{0.50}Se$	208.63	6.747	1984	3757	2218	353	176	7.368	1.814	0.878	1028
$Hg_{0.75}Zn_{0.25}Se$	221.12	7.381	1830	3488	2046	320	160	6.668	1.838	0.779	999
HgSe	232.27	7.993	1702	3267	1904	292	146	6.103	1.862	0.701	975
			1569[a]	2998[a]	212[b]	242[a*]				0.1–3.5[a*]	1072[a*]
			1635[b]	877[b]		151[b*]					
						264.30[a]					
						51.188[b]					
						231[d]					
ZnTe	224.31	5.714	2122	3881	2366	368	184	7.672	1.694	0.892	1001
$Hg_{0.25}Zn_{0.75}Te$	239.25	6.295	1919	3533	2141	326	163	6.784	1.717	0.773	960
$Hg_{0.50}Zn_{0.50}Te$	252.92	6.843	1753	3246	1957	292	146	6.098	1.736	0.681	926
$Hg_{0.75}Zn_{0.25}Te$	265.60	7.361	1615	3005	1803	265	132	5.528	1.754	0.607	896
HgTe	277.30	7.860	1510	2833	1688	244	122	5.099	1.781	0.552	877
			1518[a]	2782[a]	1693[a]	143[a*]				2.38[a*]	943[a*]
			1017[b]	1760[b]	244[b]	141[c*]					
						240.19[a]					
						55.955[b]					
						211[d]					

Experimental data ⇒ [a*]Ref. [38], [b*]Ref. [33], [c*]Ref. [32].
Previous theoretical data ⇒ [a]Ref. [55], [b]Ref. [51], [c]Ref. [57], [d]Ref. [50].

In table 5, the presented values of γ_a show that interactions between atoms in all the cubic specimens are anharmonic in nature. With enhancement in Hg-composition x in each alloy system, non-linear increase in γ_a of specimens are displayed in figure 13b.

3.2f *Thermal conductivity and melting point of the specimens:* The ability of any material to conduct heat is determined by its numerical value of thermal conductivity and it is an important parameter for thermal barrier coating applications [97,98]. According to models of Clarke [98], Liu and coworkers [99] proposed the following theoretical relation to estimate minimum thermal conductivity ($K_{\min}$) of a specimen

$$K_{\min} = k_B v_m \left(\frac{M}{n\rho N_a}\right)^{-\frac{2}{3}}. \tag{34}$$

Another important parameter, known as the melting temperature T_m (K) of a zinc-blende solid, can be estimated using elastic constant C_{11}. Fine and coworkers [100] have proposed the following empirical formula for calculation of T_m of any zinc-blende specimen

$$T_m = [553 + (5.91/\text{GPa})C_{11}]. \tag{35}$$

In table 5, we have reported the calculated minimum thermal conductivity $K_{\min}$ (W m^{-1} K^{-1}) and melting temperature T_m (K) of the specimens under consideration. With enhancement in Hg-composition x in each system, non-linear reduction in both $K_{\min}$ and T_m of the specimens are shown in figure 14a and b, respectively. Experimental $K_{\min}$ for only HgSe and HgTe as well as T_m for only HgS, HgSe and HgTe are available [38]. Our calculated $K_{\min}$ for HgSe is within the experimentally prescribed range [38], while that for HgTe is substantially underestimated with respect to the corresponding experimental data [38]. Our calculated T_m for HgS is substantially underestimated with respect to the corresponding experimental data [38], while we have observed good agreement between our calculated T_m data and corresponding experimental data for HgSe and HgTe [38]. The manipulation and control of thermal conductivity has enormous impact on a variety of technical applications including

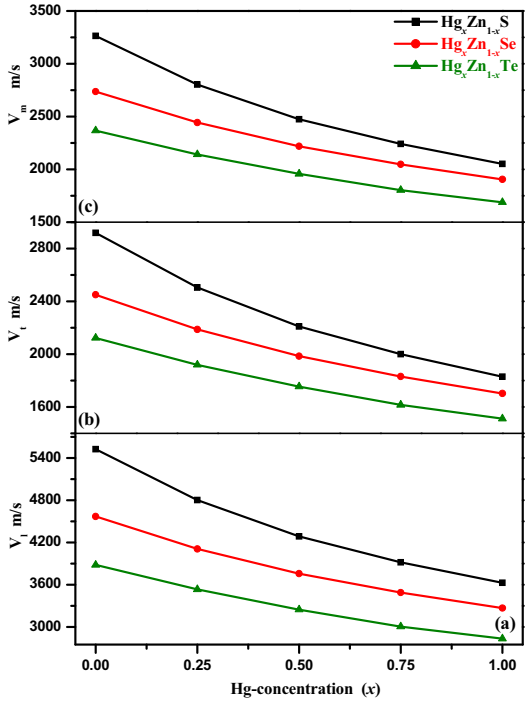

Figure 11. Concentration (x) dependence curves of calculated (**a**) v_l, (**b**) v_t, (**c**) v_m of zinc-blende $Hg_xZn_{1-x}S$, $Hg_xZn_{1-x}Se$ and $Hg_xZn_{1-x}Te$ alloys.

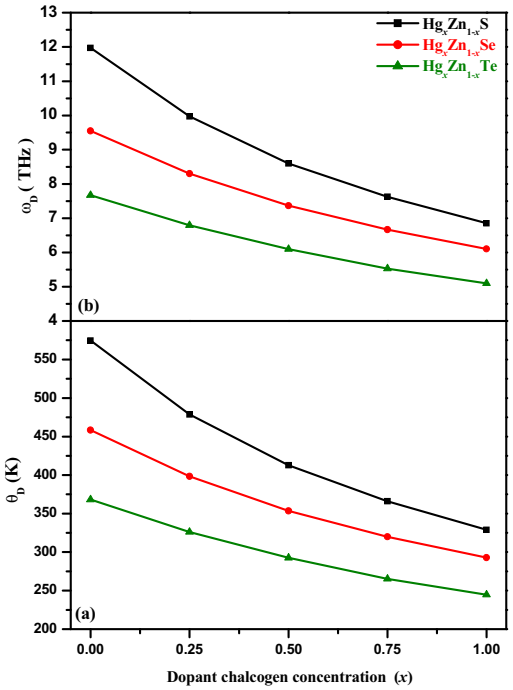

Figure 12. Concentration (x) dependence curves of calculated (**a**) θ_D, (**b**) ω_D of zinc-blende $Hg_xZn_{1-x}S$, $Hg_xZn_{1-x}Se$ and $Hg_xZn_{1-x}Te$ alloys.

thermal management of mechanical, electrical, chemical and nuclear systems. The alloys designed by us are also useful as thermal insulation materials, efficient thermoelectric materials, thermal barriers, sensors and transducers.

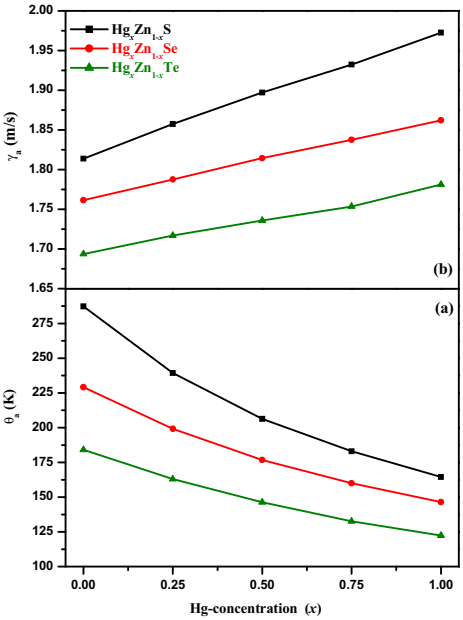

Figure 13. Concentration (x) dependence curves of calculated (**a**) θ_a (**b**) γ_a of zinc-blende $Hg_xZn_{1-x}S$, $Hg_xZn_{1-x}Se$ and $Hg_xZn_{1-x}Te$ alloys.

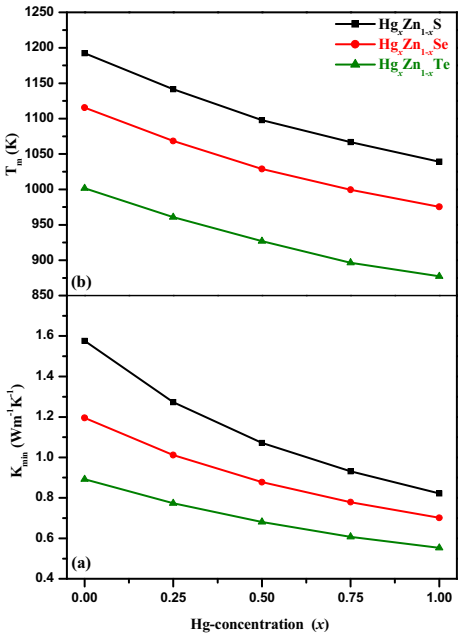

Figure 14. Concentration (x) dependence curves of calculated (**a**) $K_{\min}$, (**b**) T_m of zinc-blende $Hg_xZn_{1-x}S$, $Hg_xZn_{1-x}Se$ and $Hg_xZn_{1-x}Te$ alloys.

4. Conclusion

Elastic and thermal features of zinc-blende specimens under $Hg_xZn_{1-x}S$, $Hg_xZn_{1-x}Se$ and $Hg_xZn_{1-x}Te$ systems are calculated through density functional FP-LAPW approach. In each system, each elastic stiffness constant decreases, while elastic compliance constant increases non-linearly with

increase in Hg-composition. The mechanical stability of specimens is confirmed in terms of respective calculated elastic stiffness constants, while the dynamical stability of each specimen is confirmed with respective calculated shear constant. Hardness of each specimen is investigated by calculating the respective bulk modulus, Young's modulus and Vickers hardness. In each system, hardness of specimen decreases non-linearly with increase in Hg-concentration. Each specimen exhibits elastic anisotropy in terms of respective Zener anisotropy factor, shear modulus, Hershey's cubic equation and Lame constants. Shear modulus of the specimens in each system decreases non-linearly with the increase in Hg-concentration. Calculated Kleinmann parameter indicates that bond bending significantly dominates over bond stretching in each of the specimens. Ductility of each specimen is observed in terms of respective Pugh's ratio, Cauchy pressure and Poisson's ratio. The calculated elastic constant ratio C_{11}/C_{12} and ionic charge Z/Z_0 indicate mixed type of bonding in each specimen with dominancy of covalent nature over ionic nature in most of the specimens. Such domination of covalent bonding over ionic bonding gradually decreases with enhancement in Hg-composition in each system. Fair plasticity is observed in each specimen in terms of respective Poisson's ratio and B_0/C_{44}. In each system, calculated covalency of specimens decreases, while Philip ionicity increases with enhancement in Hg-concentration. The calculated longitudinal, transverse and mean sound velocities through the specimens as well as Debye temperature, Debye frequency, $K_{\min}$ and T_m of the specimen decrease, while their Grüneisen parameter increases non-linearly with increase in Hg-concentration in each system. Our calculated thermal conductivity of each specimen indicates their probable applications in thermal management in mechanical, electrical, chemical and nuclear systems.

Acknowledgements

We are grateful to UGC, Govt. of India for financial support to carry out this research work through financial assistance under UGC–SAP program 2016 [Ref. No. F.530/23/DRS-I/2018 (SAP-I)]. Mr Manish Debbarma is also grateful to CSIR, Govt. of India for granting him CSIR Junior Research Fellowship (NET).

References

[1] Eckelt P 1967 *Phys. Status Solidi* **23** 307
[2] Huang T L and Ruoff A L 1985 *Phys. Rev. B* **31** 5976
[3] McMahon M I, Nelmes R J, Liu H and Belmonte S A 1996 *Phys. Rev. Lett.* **77** 1781
[4] Nelmes R J and McMahon M I 1998 in *High pressure in semiconductor physics* I, T Suski and W Paul (eds) (New York: Academic Press) vol 54, p 145
[5] Shukla S and Kumar S 2012 *Pramana-J. Phys.* **78** 309
[6] Ohta T 2001 *J. Opto-Electron. Adv. Mater.* **3** 609
[7] Tanaka K 1989 *Phys. Rev. B* **39** 1270
[8] Furdyna J K 1988 *J. Appl. Phys.* **64** R29
[9] Dybko K, Szuszkiewicz W, Dynowska E, Paszkowicz W and Witkowska B 1998 *Physica B* **256** 629
[10] Arora G and Ahuja B L 2008 *Radiat. Phys. Chem.* **77** 9
[11] Szuszkiewi W 1979 *Phys. Status Solidi B* **91** 361
[12] Mycielski A, Kossut J, Dobrowolska M and Dobrowolski W 1982 *J. Phys. C* **15** 3293
[13] Gawlik K U, Kipp L, Skibowski M, Orłowski N and Manzke R 1997 *Phys. Rev. Lett.* **78** 3165
[14] Groves S H, Brown R N and Pidgeon C R 1967 *Phys. Rev.* **161** 779
[15] Mews A, Kadavanich A V, Banin U and Alivisatos A P 1996 *Phys. Rev. B* **53** R13242
[16] Bazarganipour M, Sadri M, Davar F and Salavati-Niasari M 2011 *Polyhedron* **30** 1103
[17] Esmaeili-Zare M, Salavati-Niasari M and Sobhani A 2012 *Ultrason. Sonochem.* **19** 1079
[18] Kim D W, Jang J, Kim H, Cho K and Kim S 2008 *Thin Solid Films* **516** 7715
[19] Rogach A L, Koktysh D S, Harrison M and Kotov N A 2000 *Chem. Mater.* **12** 1526
[20] Huong C N V, Triboulet R and Lemasson P 1990 *J. Cryst. Growth* **101** 311
[21] Tomashyk V, Feychuk P and Shcherbak L 2014 *Ternary alloys based on II–VI semiconductor compounds* (New York: CRC Press)
[22] Tamargo M C 2002 *II–VI semiconductor materials and their applications optoelectronic properties of semiconductors and superlattices* vol 12 (New York: CRC Press)
[23] Pawar S M, Pawar B S, Kim J H, Joo O S and Lokhande C D 2011 *Curr. Appl. Phys.* **11** 117
[24] Howes P, Green M, Johnston C and Crossley A 2008 *J. Mater. Chem.* **18** 3474
[25] Byun K, Cho K and Kim S 2010 *Mater. Chem. Phys.* **122** 246
[26] Berlincourt D, Jafee H and Shlozawa L R 1963 *Phys. Rev.* **129** 1009
[27] Lee B H 1970 *J. Appl. Phys.* **41** 2984
[28] Lee B H 1970 *J. Appl. Phys.* **41** 2988
[29] Gust W H 1982 *J. Appl. Phys.* **53** 4843
[30] Hodgins C G and Irwin J C 1975 *Phys. Status Solidi A* **28** 647
[31] Vagelatos N, Wehe D and King J S 1974 *J. Chem. Phys.* **50** 3613
[32] Alper T and Saunders G A 1967 *J. Phys. Chem. Solids* **28** 1637
[33] Lehoczky A, Nelson D A and Whitsett C R 1969 *Phys. Rev.* **188** 1069
[34] Collins J G, White G K, Birch J A and Smith T F 1980 *J. Phys. C: Solid State Phys.* **13** 1649
[35] Ford P J, Miller A J, Saunders G A, Yogurtçu Y K, Furdyna J K and Jaczynski M 1982 *J. Phys. C: Solid State Phys.* **15** 657
[36] Nelson D A, Broerman J G, Paxhia E C and Whitsett C R 1997 *Phys. Rev. Lett.* **78** 884
[37] Medelung O (ed) 1982 *Landolt Bornstein: numerical data and functional relationship in science and technology* vol 17b (Berlin: Springer)

[38] Adachi S 2009 *Properties of semiconductor alloys* (UK: Wiley)
[39] Abrikosov N Kh, Bankina V B, Poretskaya L V, Shelimova L E and Skudnova E V 1969 *Semiconducting II-VI, IV-VI and V-VI compounds* (New York: Plenum)
[40] Medelung O (ed) 1996 *Landolt Bornstein: semiconductors basic data in science & technology* (Berlin: Springer)
[41] Martin R M 1970 *Phys. Rev. B* **1** 4005
[42] Singh R K and Singh S 1987 *Phys. Status Solidi B* **140** 407
[43] Khenata R, Bouhemadou A, Sahnoun M, Reshak A H, Baltache H and Rabah M 2006 *Comp. Mater. Sci.* **38** 29
[44] Shen S G 1994 *J. Phys.: Condens. Matter* **6** 8733
[45] Soykan C, Kart S O and Cagin T 2010 *Arch. Mater. Sci. Eng.* **46** 115
[46] Hamdi I, Aouissi M, Qteish A and Meskini N 2006 *Phys. Rev. B* **73** 1
[47] Casali R A and Christensen N E 1998 *Sol. Stat. Commun.* **108** 793
[48] Bilal M, Shafiq M, Ahmad I and Khan I 2014 *J. Semicond.* **35** 0720011
[49] Wang H Y, Cao J, Huang X Y and Huang J M 2012 *Condens. Matter Phys.* **15** 13705
[50] El Haj Hassan F, Al Shafaay B, Meradji H, Ghemid S, Belkhir H and Korek M 2011 *Phys. Scr.* **84** 065601
[51] Varshney D, Shriya S and Khenata R 2012 *Mater. Chem. Phys.* **135** 365
[52] Verma A S, Singh R K and Rathi S K 2009 *Physica B* **404** 4051
[53] Al Shafaay B, El Haj Hassan F and Korek M 2014 *Comp. Mater. Sci.* **83** 107
[54] Jivani A R, Baria J K, Vyas P S and Jani A R 2016 *Adv. Mater. Res.* **1141** 153
[55] Duz I, Erdem I, Kart S O and Kuzucu V 2016 *Arch. Mater. Sci. Eng.* **79** 5
[56] Kumar V, Shrivastava A K and Jha V 2010 *J. Phys. Chem. Solid* **71** 1513
[57] Xiao-Cui Y, Jie Y, En-Jie Z and Chun-Xiao G 2011 *Phys. Status Solidi C* **8** 1703
[58] Mnasri S, Nasrallah S A, Sfina N, Bouarissa N and Said M 2009 *Semicond. Sci. Technol.* **24** 095008
[59] Hara K, Machimura H, Usui M, Munekata H, Kukimoto H and Yoshino J 1995 *Appl. Phys. Lett.* **66** 3337
[60] Deibuk V G, Dremlyuzhenko S G and Ostapov S E 2005 *Semiconductors* **39** 1111
[61] Murtaza G, Ullah N, Rauf A, Khenata R, Bin Omran S, Sajjad M *et al* 2015 *Mater. Sci. Semicond. Process.* **30** 462
[62] Debbarma M, Sarkar U, Debnath B, Ghosh D, Chanda S, Bhattacharjee R *et al* 2018 *J. Alloys Compd.* **748** 446
[63] Hohenberg P and Kohn W 1964 *Phys. Rev. B* **136** 864
[64] Kohn W and Sham L 1965 *J. Phys. Rev.* **140** A1133
[65] Andersen O K 1975 *Phys. Rev. B* **42** 3063
[66] Blaha P, Schwarz K, Madsen G H, Kbasnicka D and Luitz J 2014 *WIEN2K: an augmented plane wave plus local orbitals program for calculating crystal properties* (Austria: Technische Universität Wien)
[67] Jamal M, Asadabadi S J, Ahmed I and Aliabad H A R 2014 *Comp. Mater. Sci.* **95** 592
[68] Wu Z and Cohen E R 2006 *Phys. Rev. B* **73** 235116
[69] Kokalj A 2003 *Comp. Mater. Sci.* **28** 155
[70] Murnaghan F D 1944 *Proc. Natl. Acad. Sci. USA* **30** 244
[71] Mouhat F and Coudert F X 2014 *Phys. Rev. B* **90** 224104
[72] Adachi S 2005 *Properties of group-IV, III–V and II–VI semiconductors* (UK: Wiley)
[73] Born M and Huang K 1954 *Dynamics theory of crystal lattices* (UK: Oxford University Press)
[74] Hill R 1952 *Proc. Phys. Soc. Lond. A* **65** 349
[75] Voigt W 1889 *Ann. Phys.* **38** 573
[76] Reuss A 1929 *Z. Angew. Math. Phys.* **9** 49
[77] Ledbetter H M 1973 *J. Appl. Phys.* **44** 1451
[78] Hashin Z and Shtrikman S 1962 *J. Mech. Phys. Solids* **10** 343
[79] Teter D 1998 *MRS Bull.* **23** 22
[80] Chen X Q, Niu H Y, Li D Z and Li Y Y 2011 *Intermetallics* **19** 1275
[81] Frantsevich I N, Voronov F F and Bokuta S A 1983 *Elastic constants and elastic moduli of metals and insulators handbook* (Kiev: Naukova Dumka)
[82] Kleinman L 1962 *Phys. Rev.* **128** 2614
[83] Vitos L, Korzhavyi P A and Johansson B 2003 *Nat. Mater.* **2** 25
[84] Pugh S F 1954 *Philos. Mag.* **45** 823
[85] Pettifor D G 1992 *Mater. Sci. Technol.* **8** 345
[86] Li S, Li S and Ju X 2017 *J. Alloys Compd.* **695** 2916
[87] Hershey A V 1954 *J. Appl. Mech.* **21** 236
[88] Potter R Y 1957 *J. Phys. Chem. Solid* **3** 223
[89] Mavroides J G and Kolesar D F 1964 *Solid State Commun.* **2** 363
[90] Kumazaki K 1976 *Phys. Status Solidi A* **33** 615
[91] Phillips J C 1970 *Rev. Mod. Phys.* **42** 317
[92] Hiadsi S, Bouafia H, Sahli B, Abidri B, Bouaza A and Akriche A 2016 *Solid State Sci.* **58** 1
[93] Zhang X D, Hou Z F, Jiang Z Y and Hou Y Q 2011 *Physica B* **406** 2196
[94] Huang W and Yang L 2015 *Can. J. Phys.* **93** 1
[95] Jia T, Chen G and Zhang Y 2017 *Phys. Rev. B* **95** 155206
[96] Belomestnykh V N 2004 *Tech. Phys. Lett.* **30** 91
[97] Clarke D R and Phillpot S R 2005 *Mater. Today* **8** 22
[98] Clarke D R 2003 *Surf. Coat. Technol.* **67** 163
[99] Liu B, Wang J Y, Li F Z and Zhou Y C 2010 *Acta Mater.* **58** 4369
[100] Fine M E, Brown L D and Marcus H L 1984 *Scr. Metall.* **18** 951